Report
R-15-14
March 2015

Grain boundary sliding in phosphorus alloyed oxygen-free copper under creep

Rui Wu
Joacim Hagström
Rolf Sandström

SVENSK KÄRNBRÄNSLEHANTERING AB

SWEDISH NUCLEAR FUEL
AND WASTE MANAGEMENT CO

Box 250, SE-101 24 Stockholm
Phone +46 8 459 84 00
skb.se

SVENSK KÄRNBRÄNSLEHANTERING

ISSN 1402-3091
SKB R-15-14
ID 1479284
March 2015

Grain boundary sliding in phosphorus alloyed oxygen-free copper under creep

Rui Wu, Joacim Hagström, Rolf Sandström
Swerea KIMAB

Keywords: Grain boundary sliding, EBSD examination, Subgrain, Creep, Constant loading rate, Interruption, Cu-OFP.

Abstract

Two creep tests have been performed at constant loading rate at 125°C for oxygen free phosphorus containing pure copper, Cu-OFP. The tests were interrupted after certain strains and the amount of grain boundary sliding (GBS) was measured on flat polished surfaces. Displacements across grain boundaries were recorded at scratch marks that had been introduced before the start of the tests. The amount of GBS displacement was found to be about 20 to 65 μm per unit plastic strain. This is of the same order of magnitude as for previously published tensile tests (150 and 200°C) and short time creep tests (400 to 600°C).

The technical interest of GBS is due to the fact that it introduces creep damage. GBS gives rise to nucleation of creep cavities that grow and link during creep and eventually lead to creep rupture. In the present study, creep damage in the form of wedge and intergranular microcracks was found in the interrupted-restarted-interrupted test specimen after about 20% creep strain. Very few GBS sliding events were observed, which may contribute to the excellent creep ductility of Cu-OFP.

The deformation of the microstructure was followed with the help of electron backscatter diffraction (EBSD). Pronounced rotation of the crystal grains as well as lattice rotations at twin- and grain boundaries were observed. Multiple slip systems were developed in many grains. Subgrains developed along the slip bands.

Contents

1 Introduction

In Sweden the spent nuclear fuel is planned to be disposed underground by encapsulating in cast iron inserts enclosed by copper canisters (Rosborg and Werme 2008). The copper canisters will be made of phosphorus alloyed oxygen-free copper (Cu-OFP). Due to external hydrostatic pressure, the copper canister will be exposed to creep deformation (Jin and Sandström 2008, 2009, Sandström 2012).

During creep, shear stresses will force the grains to slide against each other, so-called grain boundary sliding (GBS). GBS occurs along the grain boundaries as a bulk movement of two grains. GBS is one of the deformation mechanisms of materials at elevated temperature and low strain rate. GBS can give a significant contribution to the overall creep strain. The main mechanism of GBS is the combined motion of dislocations in and around the grain boundaries by glide and climb (Sheikh-Ali 2001). GBS takes place discontinuously with time and the amount of shear displacement is not uniform along the grain boundary.

An important effect of GBS is in the process of creep failure in terms of cavity initiation leading eventually to final rupture. It has been shown that cavities were developed by GBS on the grain boundaries of oxygen-free, high-conductivity copper specimens in the tertiary creep stage at 415°C (Davies and Williams 1969). Langdon found that cavities are especially prevalent in pure copper at elevated temperatures and cavity nucleation is inhomogeneous (Langdon 1993). However, there are many boundaries where no cavities are detected at all. It has been suggested that low angle and twin boundaries are creep cavitation resistant (Tan 1997).

Observations and measurements on the creep strain attributable to GBS have frequently been performed on the specimen surface using scribe lines or micro-grid (see for example Harper et al. 1958) and more recently using focused ion beam (Koike et al. 2003, Rust and Todd 2011). Using scribe lines on a polished and etched surface, the shear offset under application of stress σ can be observed and measured where the line crosses the grain boundary, see Figure 1-1. Pettersson (2010) has used this technique to evaluate GBS in Cu-OF and Cu-OFP in tensile tests for up to 4% plastic deformation at temperatures up to 200°C. The larger the plastic deformation, the larger was the mean sliding distance.

Recently, Sandström and Wu (2013) have proposed a so-called double ledge model to explain why the nucleation rate of creep cavities is proportional to the creep strain rate which is in turn related to GBS rate. The model is based on the assumption that phosphorus agglomerates at the grain boundaries, retards the local deformation and thereby reduces the formation and growth of cavities.

The longest testing times in Pettersson's work for GBS measurements were 3 h. GBS measurements after creep tests for Cu-OF have also been performed by Ayensu and Langdon (1996). In this case the longest testing time was 5 h. In the model for cavity nucleation and growth of Sandström and Wu, a rupture time of 10,000 h was considered It is therefore of importance to measure GBS during long-term creep testing.

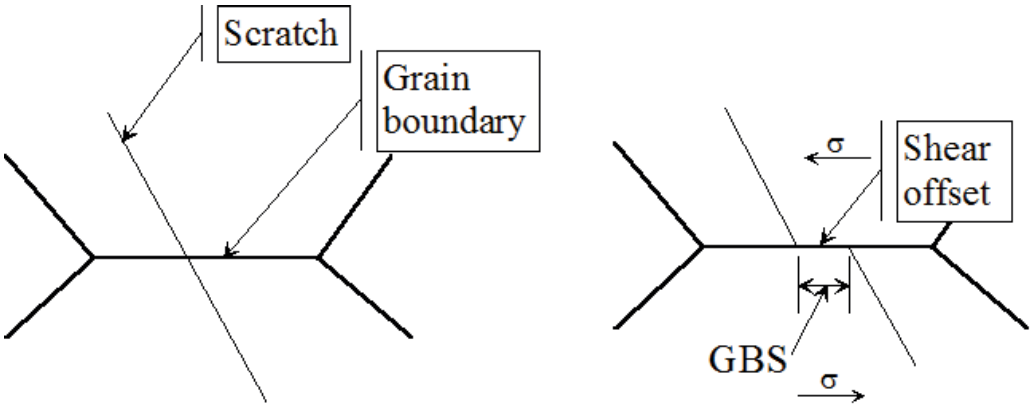

Figure 1-1. *Schematic illustration of observation and measurement of GBS.*

2 Purpose of the project

The purposes of the present work were to

1) carry out creep test with controlled loading rate and controlled deformation,
2) characterise microstructural features in terms of deformation,
3) measure grain boundary sliding quantitatively and compare with previous results.

3 Materials and experiments

3.1 Material

The Swedish Nuclear Fuel and Waste Management Co (SKB) provided test material, which is a phosphorus alloyed oxygen-free copper (Cu-OFP). The material was cast in vacuum and hot forged. The chemical composition is given in Table 3-1. The microstructure of the investigated Cu-OFP is exhibited in Figure 3-1. The microstructure had mixed grain sizes with a mean grain size of 150 µm.

Table 3-1. Chemical composition of the investigated Cu-OFP in wt. ppm, except for Cu (wt%).

Cu	P	Ag	Al	As	Bi	Cd	Co	Cr	Fe	H	
99.991	66	7.7	<0.08	0.3	<0.3	<0.4	<0.1	<0.05	0.8	0.58	
Mn	**Ni**	**O**	**Pb**	**S**	**Sb**	**Se**	**Si**	**Sn**	**Te**	**Zn**	**Zr**
<0.1	1.3	3.1	<0.7	3	<1	<0.7	<0.2	0.7	<2	<0.1	<0.2

3.2 Round bar specimen with parallel planes

Round bar specimens were first manufactured. The dimension of the bar specimens is given in Figure 3-2. Two parallel planes were then machined to facilitate observation and measurement of GBS, see Figure 3-3.

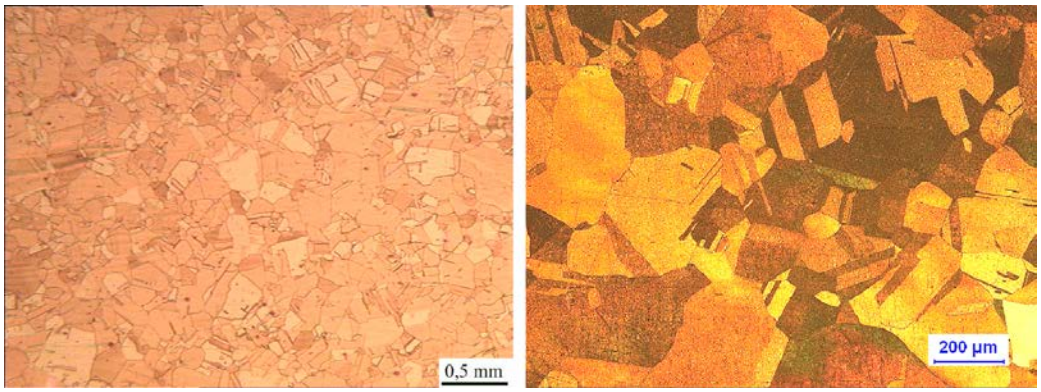

Figure 3-1. *Investigated Cu-OFP.*

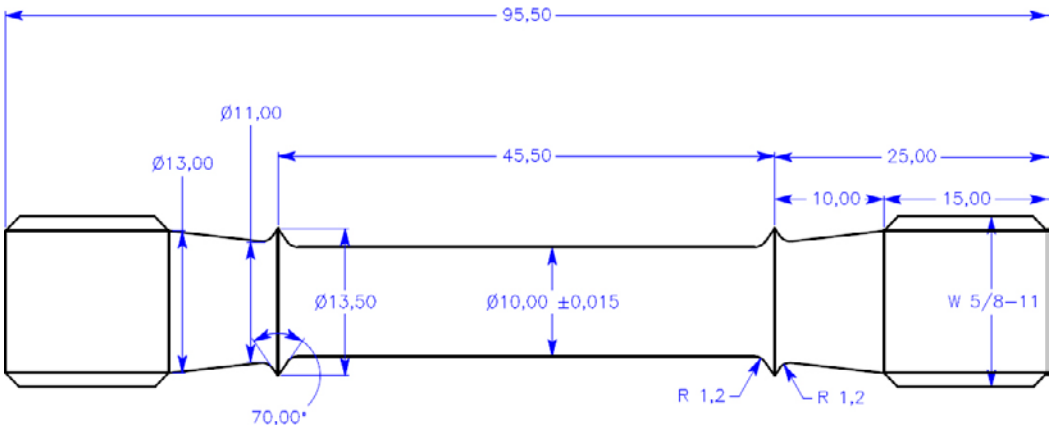

Figure 3-2. *Round bar specimen.*

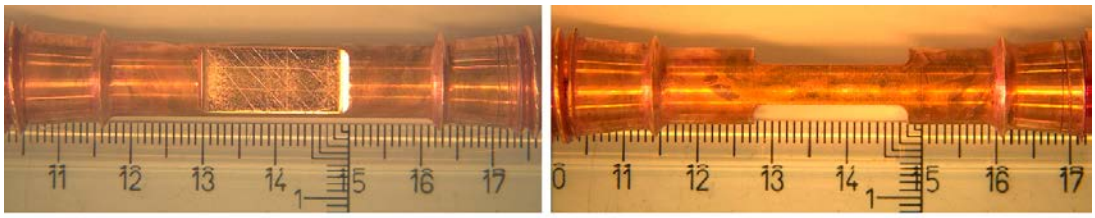

Figure 3-3. *Round bar specimens with two parallel planes.*

3.3 Specimen preparation prior to creep testing

Before creep testing, the planar surfaces were ground and polished to 0.25 µm, and finally etched in a solution containing 40 g CrO_3, 7.5 g HN_4Cl, 50 ml H_2SO_4, 50 ml HNO_3 and 1,900 ml H_2O. Microstructure examination was then carried out on the etched planes using a Leica light optical macroscope (LOM), the Leica DM IRM, and a scanning electron microscope the Leo1530 upgraded to a Zeiss Supra 55 with a field emission-gun (FEG-SEM). Grains and their boundaries on the etched planes are shown in Figure 3-3a and Figure 3-4. On the etched planes, scratches were randomly added to be able to follow the movement at the grain boundaries. Scratches were made by sharp knife with an angle either vertical to or 45° off the stress axis.

3.4 Creep testing with constant loading rate

Creep testing was conducted on test rigs using a step motor actuating load through a gearbox and an angled gear, see Figure 3-5. A load cell is incorporated in the load chain in this test setup and the step motor is controlled by feedback from the load cell. The load during the test was regulated within 1 N of target load, fulfilling the requirement of ASTM E139-2011 standard. An in-house developed programme controls load increment at a given loading rate. In the present case the loading rate was constant. The furnace is of hot air type and temperature is controlled within ±1°C.

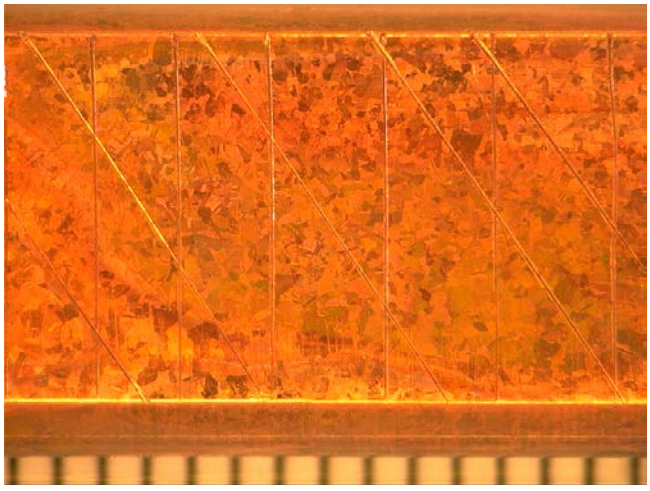

Figure 3-4. *Etched and scratched plane on which GBS was observed and measured.*

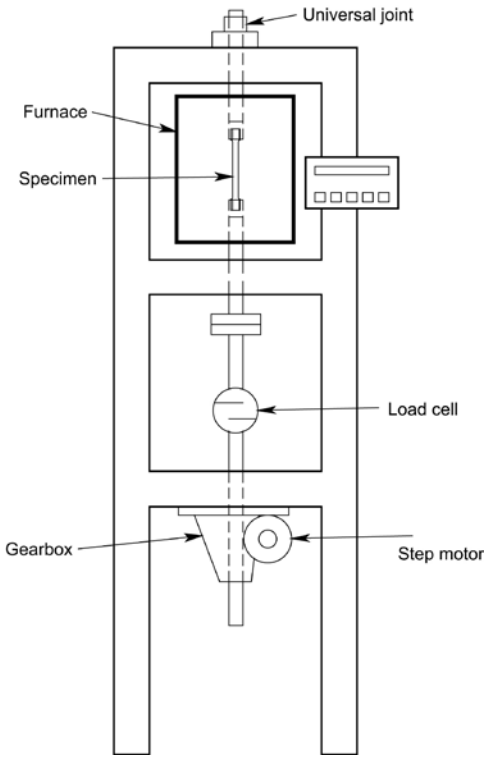

Figure 3-5. *Schematic drawing of load controlled creep test rig (after Andersson-Östling and Sandström 2011).*

Two creep tests with controlled (constant) loading rate were carried out at 125°C. This is expected to simulate the loading of the canister during the initial period in the repository. The test matrix is given in Table 3-2. The test using specimen REF40-2 with constant loading rate of 12 N/h was interrupted after 307 h to observe and measure GBS. The test was then restarted from zero load and interrupted after a total of 502 h. The test using specimen REF40-3 with constant loading rate of 2.82 N/h was interrupted after 1,096 h. After interruption, GBS on both specimens was observed and measured using light optical microscopy (LOM) and a field emission gun-scanning electron microscope (FEG-SEM).

Silicon was applied on the planar surfaces to provide protection against oxidation. The silicon was removed before observation of GBS.

Table 3-2. Creep testing matrix

Specimen	Load bearing area (mm^2)	Constant loading rate (N/h)	Corresponding stress increasing rate (MPa/h)	Comments
REF40-2	50.37	12	0.238	Interrupted after 307 h to observe and measure GBS, then restarted the test from zero load to 502 h before second interruption.
REF40-3	50.23	2.82	0.056	Interrupted after 1,096 h.

3.5 Post test metallographic examination

Post test metallographic examinations were performed using LOM and FEG-SEM. Electron backscatter diffraction (EBSD), also known as backscatter Kikuchi diffraction (BKD), was used to study crystal orientation, grain boundary deformation and slip system activity. In crystal orientation mapping a grain is defined if the boundary misorientation indicated by colour mapping is larger than a certain threshold value, e.g. 5 or 15°.

A well prepared specimen is a prerequisite to obtain a good diffraction pattern by EBSD. The surface of the specimen must be sufficiently smooth to avoid forming shadows on the diffraction pattern from other parts of the specimen. In the present case, electrolytic polishing at room temperature was applied to remove distorted surface layer and to smoothen the surface where EBSD examination was performed. Before electrolytic polishing, the specimen was sealed so that only an approximately 5×5 mm^2 area was polished, see Figure 3-6. The electrolyte consisted of 250 ml 85% H_3PO_4 and 250 ml distilled water with a few drops of ethyl alcohol and propyl alcohol. The voltage was 1.7 V. The polishing time was about five minutes. During polishing the electrolyte was stirred continuously. Immediately after the electrolytic polishing, the surface was cleaned and rinsed with absolute alcohol. Alcohol was then repeatedly blown off with hot air to remove residues of solvent and other dirt.

The EBSD specimen was tilted 70° relative to the normal incidence of the electron beam to optimise both the contrast in the diffraction pattern and the fraction of electrons scattered from the specimen.

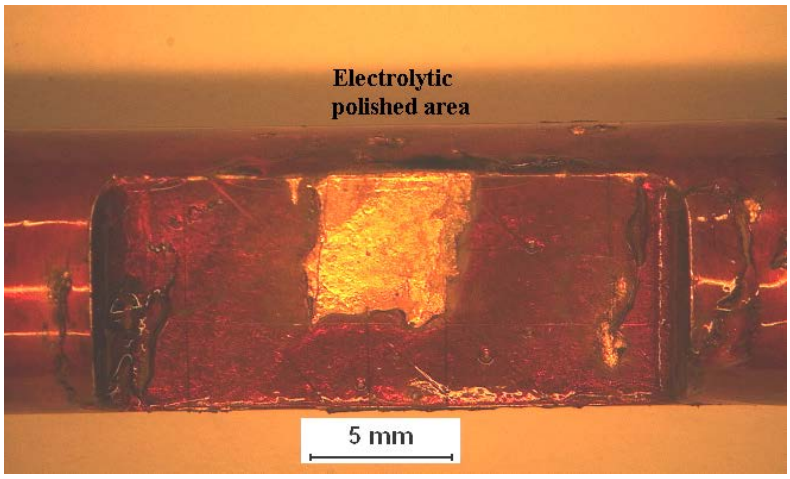

Figure 3-6. *Specimen REF40-2. Dark area was sealed and light area was electrolytically polished.*

4 Results

4.1 Creep testing

The creep testing results at 125°C are given in Table 4-1. The test using specimen REF40-2 with a constant loading rate of 12 N/h was interrupted after 307 h. At interruption, the stress and the strain were 73.7 MPa and 3.36%, respectively. Stress and strain as a function of time to 307 h are presented in Figure 4-1. It can be seen that stress increases at a constant rate, which is a direct consequence of the constant loading rate, see the red line in Figure 4-1. A non-linear relation between strain and time is observed, see the blue line in Figure 4-1. After commencement of test, the strain increase with time is reduced. A minimum strain rate of about 1×10^{-4}/h is found between 110–130 h (corresponding to a strain of about 1.6% and a stress of about 35 MPa, see Figure 4-2). Then, the strain increases faster with time. A maximum strain rate of about 3×10^{-3}/h is recorded just before the interruption. The stress-strain relation is exhibited in Figure 4-2. From Figure 4-1 and Figure 4-2 it is seen that there is an inflection point at about 30 MPa, over which the strain rate increases with increasing time and stress.

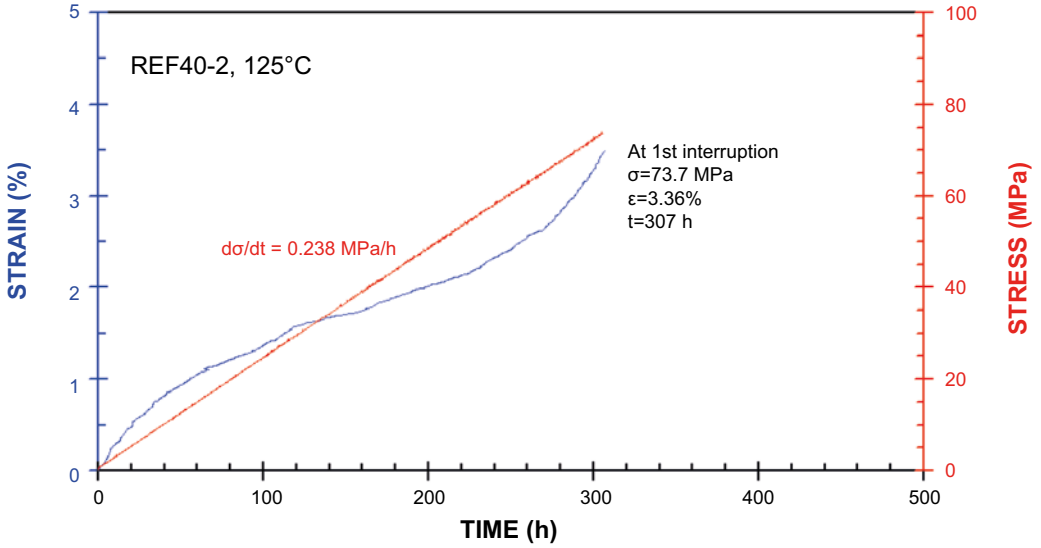

Figure 4-1. *Stress (red line) and strain (blue line) as a function of time for the test with a constant loading rate of 12 N/h. The test was interrupted after 307 h.*

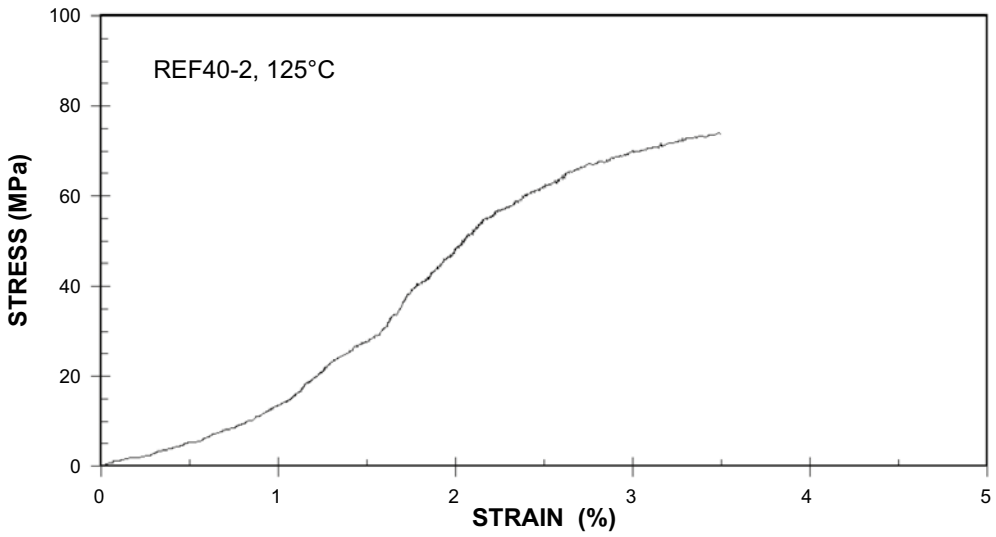

Figure 4-2. *Stress versus strain for the test with a constant loading rate of 12 N/h. The test was interrupted when the stress and the strain were 73.7 MPa and 3.36%, respectively.*

Table 4-1. Creep testing results at 125°C.

Specimen	Constant loading rate (N/h)	Corresponding stress increasing rate (MPa/h)	At interruption		
			Time at interruption (h)	Stress (MPa)	Strain (%)
REF40-2	12	0.238	307 (1st interruption)	73.7	3.36
			502 (2nd interruption)	46.8	20.8
REF40-3	2.82	0.056	1,096	61.4	5.04

This test with the specimen REF40-2 was then restarted from zero load at the same loading rate as before the interruption and continued until a total testing time of 502 h had been reached. At the 2nd interruption, the stress was 46.8 MPa and the accumulated strain 20.8%, see also Table 4-1. Stress and strain as a function of time are shown in Figure 4-3 for the whole test. It is apparent that the strain increases faster after restart. This can be also verified by plotting the stress-versus strain, see Figure 4-4, where the strain increases faster with increasing stress after restart. The strain rate at the 2nd interruption had doubled in comparison to that at the 1st interruption.

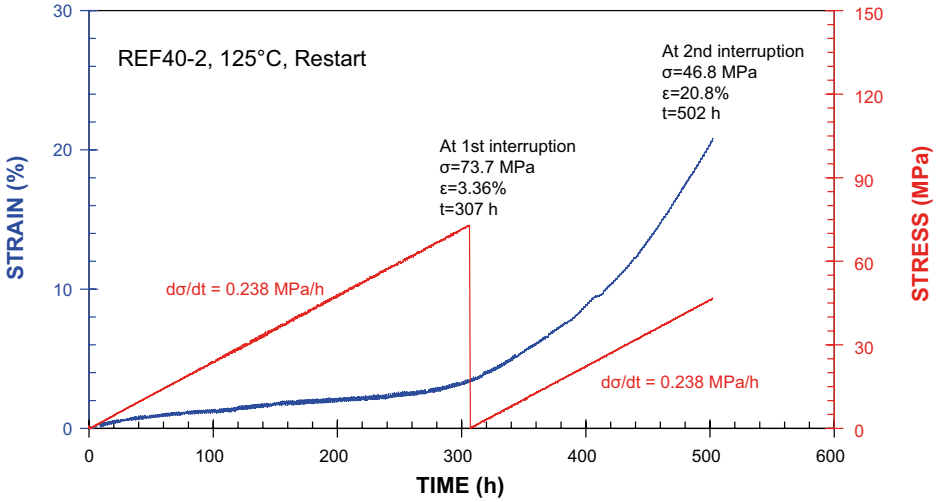

Figure 4-3. Stress (red line) and strain (blue line) as a function of time for the test with a constant loading rate of 12 N/h. The test was first interrupted after 307 h, then restarted with the same loading rate and finally stopped after 502 h.

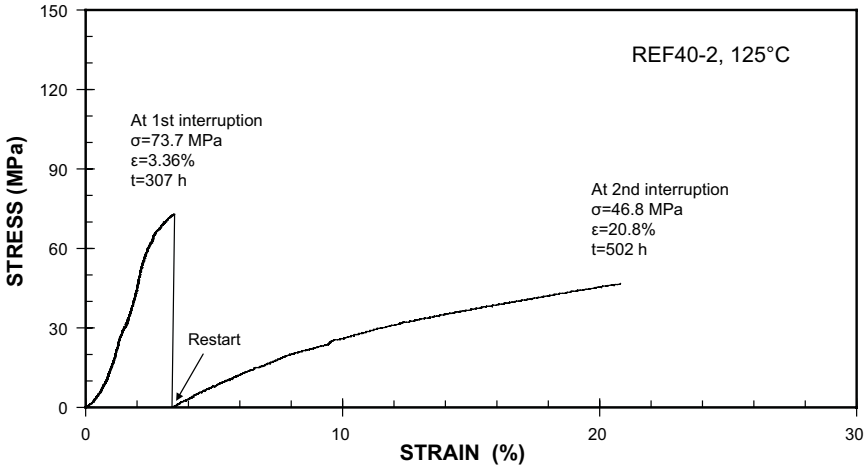

Figure 4-4. Stress versus strain for the whole test with a constant loading rate of 12 N/h. At the final interruption the stress and strain were 46.8 MPa and 26.8%, respectively.

Stress and strain as a function of time for the test using specimen REF40-3 with a constant loading rate of 2.82 N/h is presented in Figure 4-5. It can be seen again that the stress shows a constant increase with time. This time the rate is 0.056 MPa/h, see the red line in Figure 4-5. A non-linear relation between strain and time is observed, see the blue line in Figure 4-5. The strain increase slows down with time after beginning of test. A minimum strain rate of about 2×10^{-5}/h is found after 400–500 h (corresponding to a strain of about 1.6%, and a stress of about 25 MPa, see Figure 4-6). Then, the strain increases faster with time. A maximum strain rate of about 1×10^{-4}/h is recorded at interruption. The stress-strain relation is shown in Figure 4-6. There is a inflection point at about 30 MPa, over which a faster increase in strain is observed with increasing stress.

Strain as a function of time is shown in Figure 4-7 for the two tests. The strain clearly increases with increasing loading rate dσ/dt. The 'turning point' over which the strain increases faster occurs early at a larger dσ/dt. The stress-strain relation for two tests with different dσ/dt is demonstrated in Figure 4-8. The red line represents a constructed strain-stress relation after restart with an addition of the stress at interruption. The strain-stress relation is also dσ/dt dependent. At the same stress, lower dσ/dt gives larger strain. The 'turning point' over which the strain increases faster appears at lower stress at lower dσ/dt.

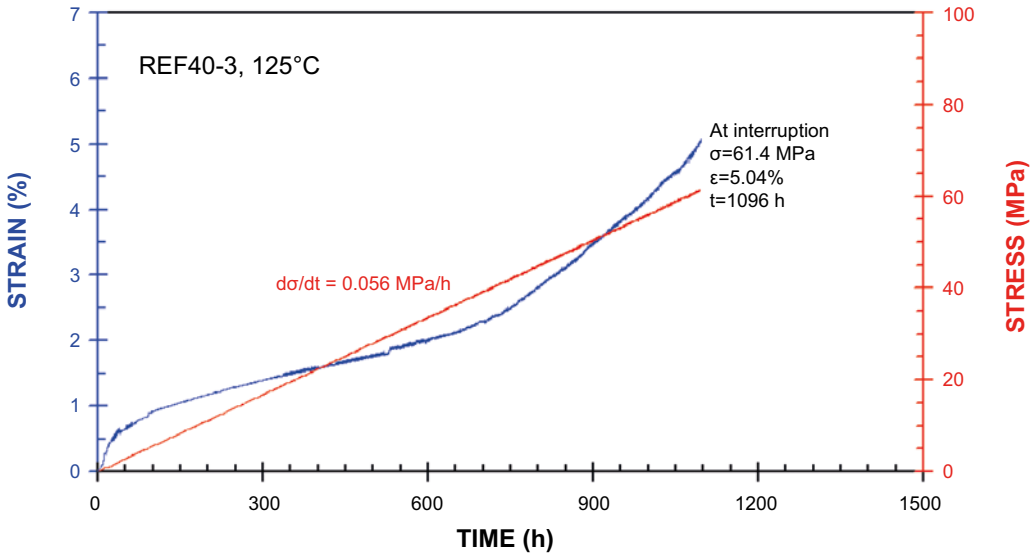

Figure 4-5. *Stress (red line) and strain (blue line) as a function of time for the test with a constant loading rate of 2.82 N/h. The test was interrupted after 1,096 h.*

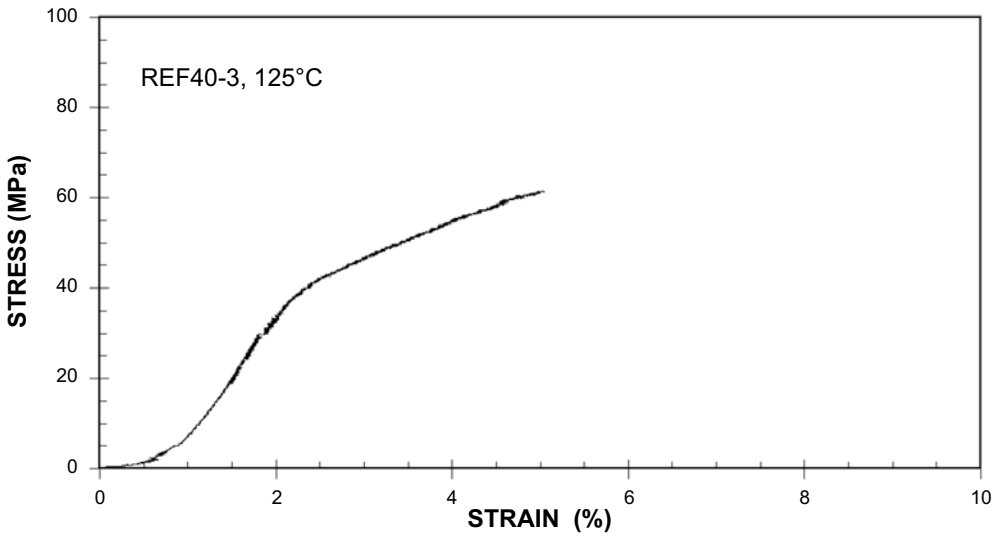

Figure 4-6. *Stress versus strain for the test with a constant loading rate of 2.82 N/h. The test was interrupted at which the stress and the strain are 61.4 MPa and 5.04%, respectively.*

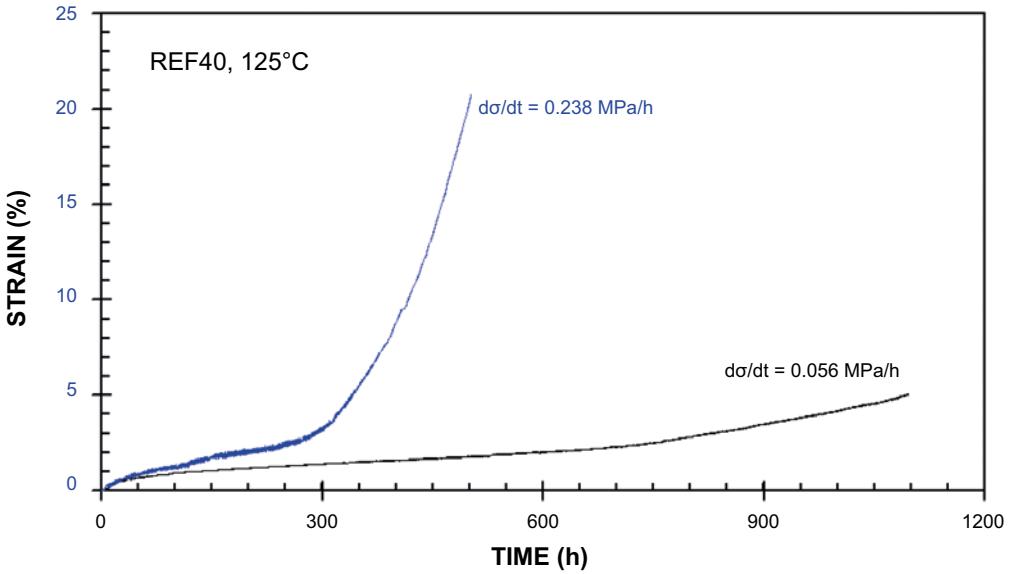

Figure 4-7. *Strain as a function of time for two tests with different stress (load) increasing rate.*

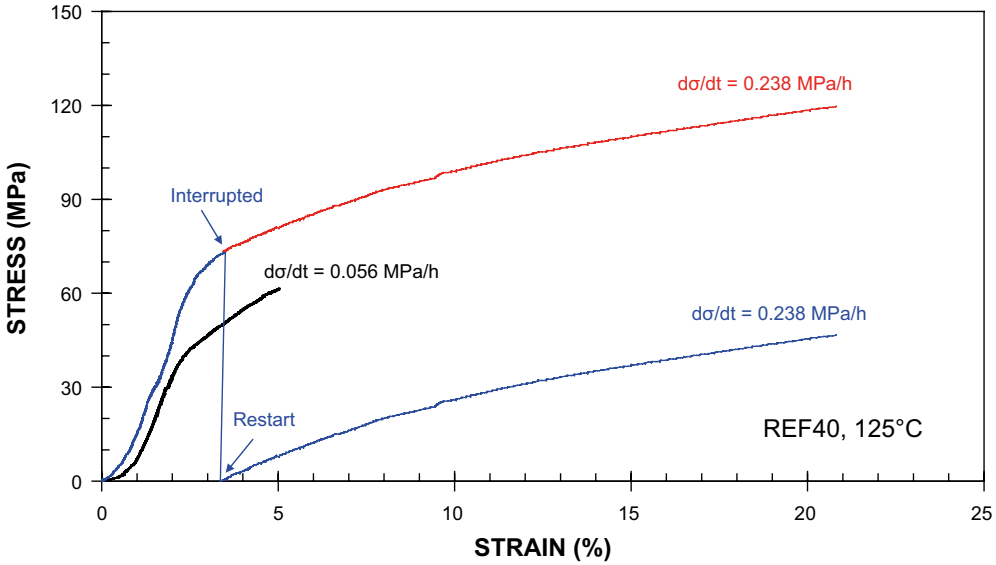

Figure 4-8. *Stress versus strain for the two tests with different loading rate. The red line represents a constructed strain-stress relation after restart with an addition of the stress at interruption, see also Figure 4-3.*

4.2 Analysis of strains and deformation using EBSD

4.2.1 Specimen REF40-2 after 502 h and 20.8% strain

Figure 4-9a shows EBSD "band slope" (BS) results; grain boundaries, twin boundaries and slip bands are well displayed. Band slope describes the maximum intensity gradient at the margins of the Kikuchi bands in EBSD with a stationary beam. The material has been deformed significantly and it can be seen that many grains have developed multiple slip systems. In Figure 4-9b crystal orientations are coloured according to an inverse pole figure (IPF) in the Y direction. The shifting colours within grains show that rotation of the crystal lattice has happened. The graph shows one example where continuous rotation within a grain caused more than 10° difference from start to end of the line. Figure 4-10a gives grain boundaries with a misorientation between 1.5° and 15°. Figure 4-10b shows grain boundaries with larger misorientation than 15° and twin boundaries (60° <111>). Many obvious original twins (straight lines) do not show a twin relation, due to lattice rotations caused by the plastic deformation.

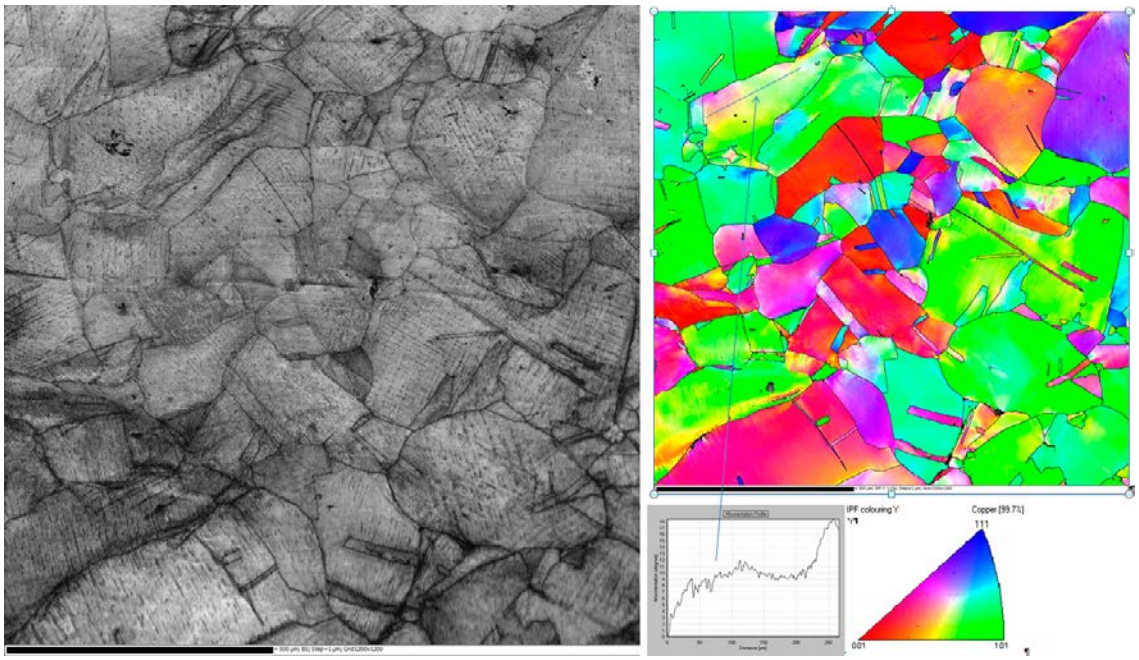

Figure 4-9. *a) EBSD "band slope" and b) crystallographic orientations. Specimen REF 40-2 after 502 h. The black bar at the bottom of the figures represents a length of 500 µm.*

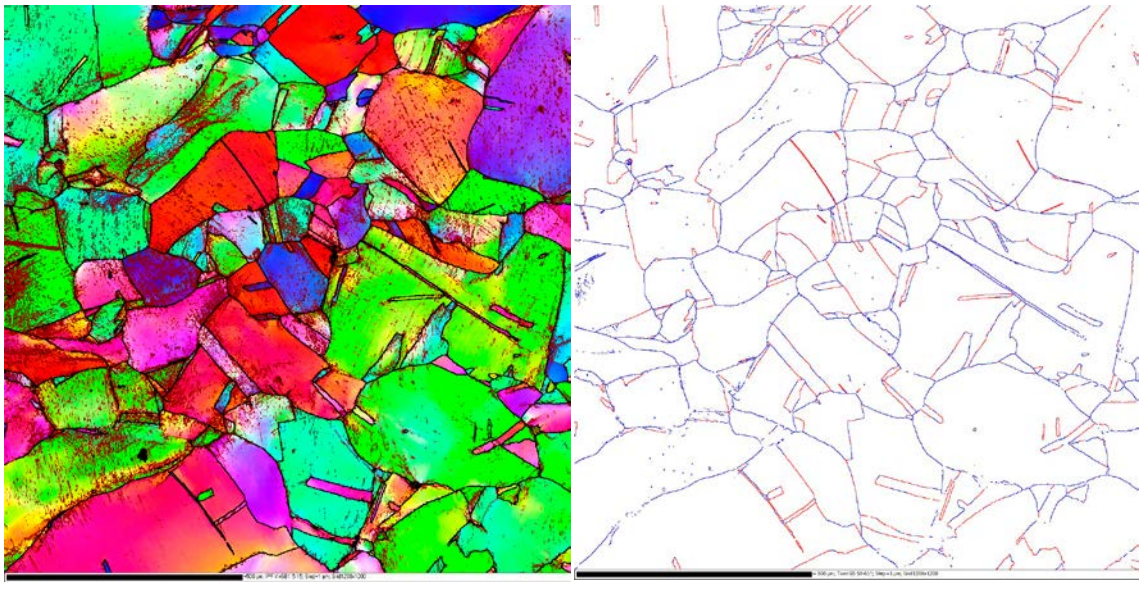

Figure 4-10. *Crystal orientations coloured according to inverse pole figure (Y). a) Grain boundaries 1.5–15 (thin) and >15° (thick). b) Grain boundaries <15° (blue), >15° (red), and twins 60°<111> (59°–61°)(red). Specimen REF 40-2 after 502 h. The black bar at the bottom of the figure represents a length of 500 µm.*

Analysis of the deformation induced by dislocation movement using the "local misorientation" component in the analysis software "Tango" was performed. The step length during EBSD analysis was 1 µm in this analysis. Figure 4-11a gives a plot of the average misorientation for each pixel and its 8 closest neighbours. Figure 4-11b shows details of Figure 4-11a with very clear slip bands in two slip systems. Misorientations between pixels along a line is also included showing misorientations around 2–3°. It also clearly demonstrates that dislocation pile-ups induce lattice rotations at twin- and grain boundaries.

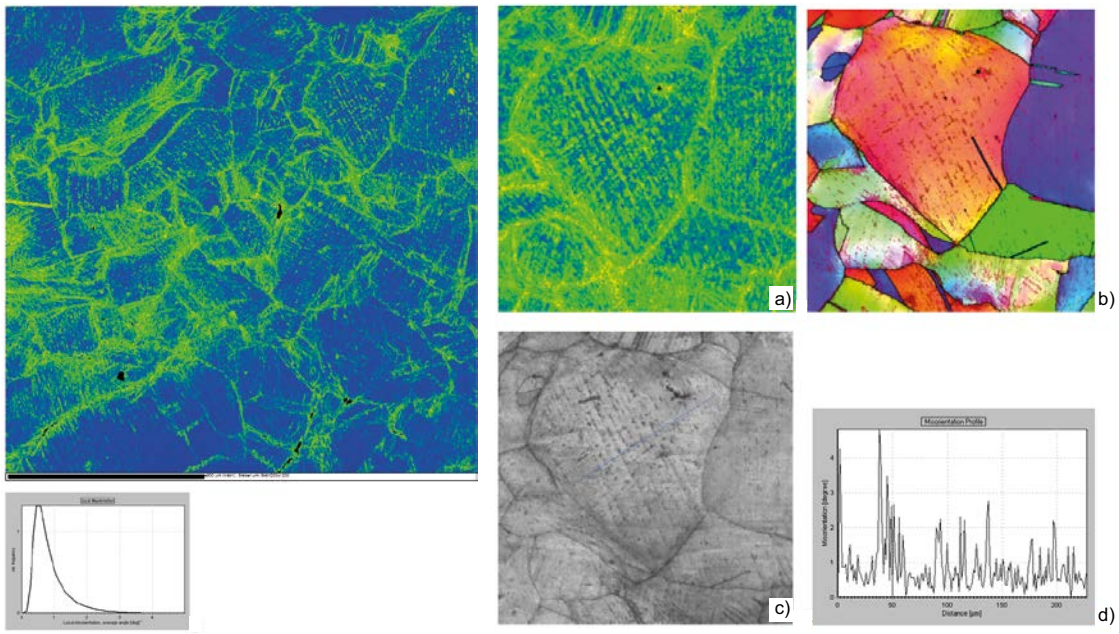

Figure 4-11. *(i) Local misorientation analysis showing localised deformation in slip bands and dislocation pile ups at grain boundaries. (ii) Details from (i); a) Local misorientation analysis. b) IPF colouring and grain boundaries < 15° (thin) and > 15° (bold). c and d)) Band slope with misorientations between pixels along the line. Specimen REF 40-2 after 502 h.*

4.2.2 Specimen REF40-3 after 1,094 h and 5.04% strain

Figure 4-12a show EBSD "band slope" (BS) results. Grain boundaries, twin boundaries and slip bands are again clearly displayed. In Figure 4-12b crystal orientations were coloured according to inverse pole figure in the Y direction and the shifting colours within grains show rotation of the crystal lattice. The apparent deformation in Figure 4-12 is clearly less than in Figure 4-9 as it should be due to the lower creep deformation in specimen REF 40-3.

Analysis of deformation induced by dislocation movement using the "local misorientation" component in "Tango" was performed. The step length during EBSD analysis was 1 µm in this analysis. Figure 4-13 shows average misorientations for each pixel and its 8 closest neighbours.

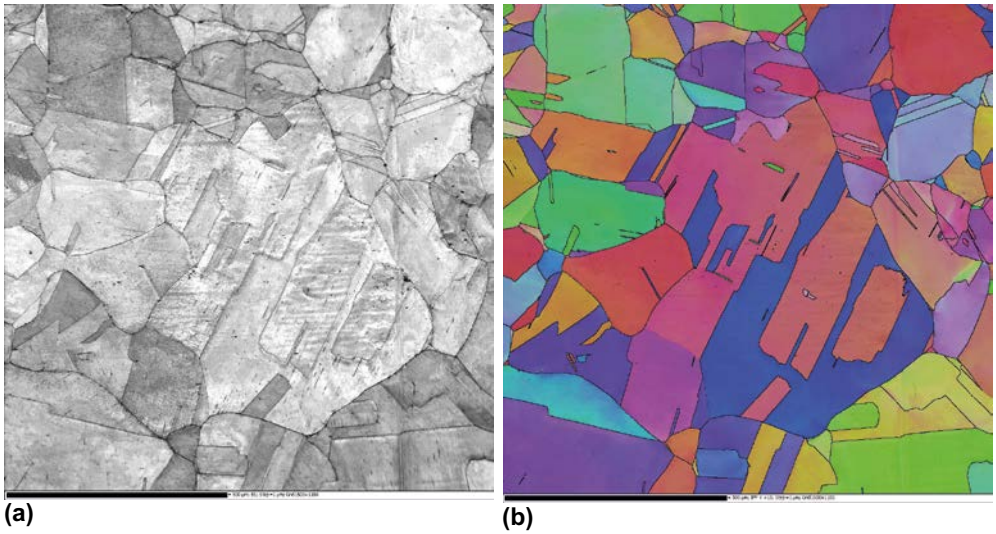

Figure 4-12. *a) EBSD "band slope" and b) crystallographic orientations. Specimen REF 40-3 after 1,094 h. The black bar at the bottom of the Figure represents a length of 500 µm.*

Figure 4-14 shows details of Figure 4-13 with clear slip bands and their interactions with grain boundaries and triple points. Figure 4-15 shows crystal orientations according to IPF X and the figures clearly demonstrate plastic deformation close to triple points indicating GBS.

The specimen was deformed significantly but somewhat differently compared to the specimen REF 40-2. It can be seen that subgrains have developed along the slip bands in many grains (Figure 4-13b). Multiple slip systems were not seen as frequently as in REF 40-2.

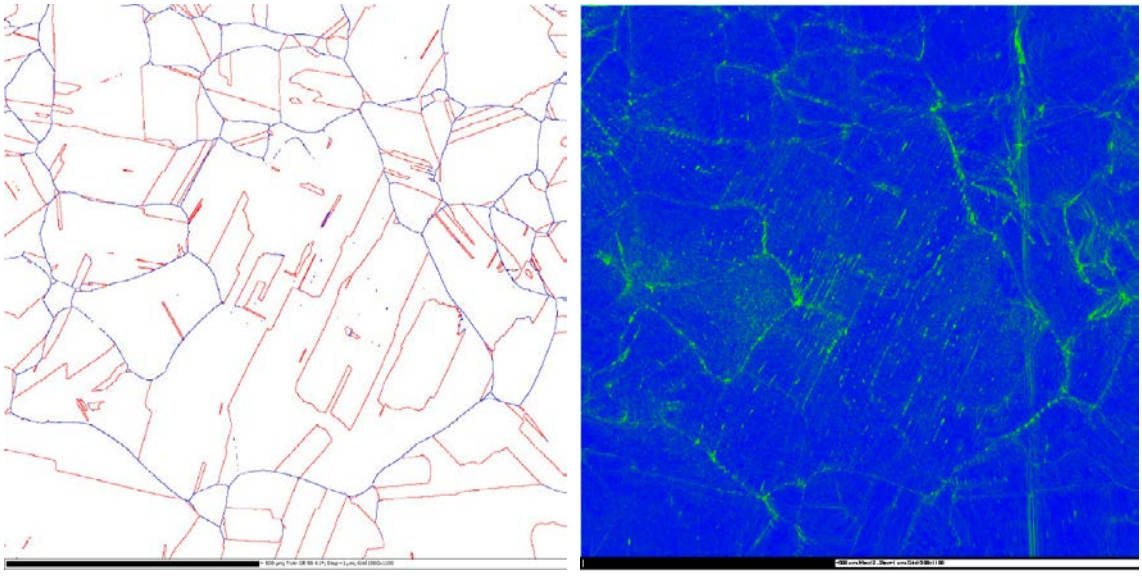

Figure 4-13. *a) Grain boundary misorientations <15° (blue), >15° (red), and twins 60°<111> (59°–61°) (red). b) Local misorientation analysis using 3×3 matrix. Average misorientation for each pixel to the 8 closest neighbours. Plastic deformation in slip bands, increasing deformation at grain boundaries, and triple points where dislocations pile ups are built up. Specimen REF 40-3 after 1,094 h. The black bar at the bottom of the Figure represents a length of 500 µm.*

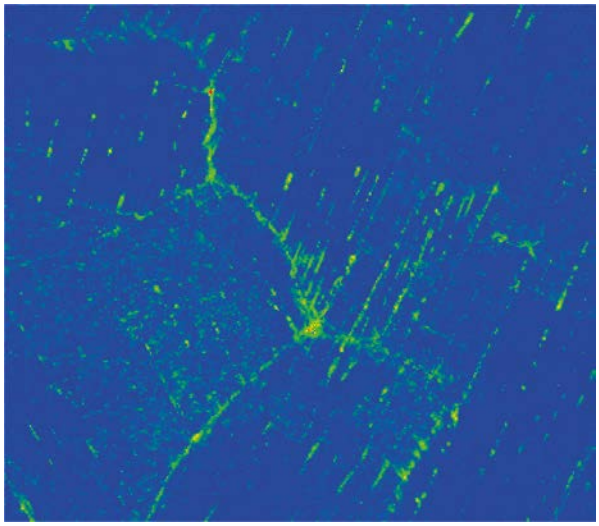

Figure 4-14. *Detail from Figure 4-13. Local misorientation analysis using 3×3 matrix. Plastic deformation in slip bands, increasing deformation at grain boundaries triple points where dislocations pile ups are built up.*

Figure 4-15. *Triple points with crystal rotation in the close vicinity, and examples of severe plastic deformation.*

4.3 Analysis of strains and deformation using SEM imaging

SEM images taken from the specimen REF40-2 show that, after the 1st interruption at t = 307 h and ε = 3.36%, many slips bands have been generated on different slip planes, see Figure 4-16. There are many cross-slip bands, see Figure 4-16a. Slip planes bend as they meet twins. Slip bands take different orientations in different grains, see Figure 4-16b. The strong relief demonstrates bulk movement of neighbouring grains.

GBS has been measured on the surface of the specimen REF40-2 after the 1st interruption at t = 307 h and ε = 3.36%, see Figure 4-17. The amount of GBS varies slightly from position to position. The measured GBS is from 0.706 µm to 1.031 µm.

After the 2nd interruption at t = 502 h and ε = 20.8%, the GBS has been measured again on the surface of the specimen REF40-2, see Figure 4-18. The amount of GBS has increased comparing to that after the 1st interruption, although the GBS is not measured at the same positions as those after 1st interruption. GBS as large as 5 µm was measured.

Intergranular microcracks are observed on the surface of the specimen REF40-2 after 2nd interruption, see Figure 4-19. Typical size of the microcracks is about 20 µm.

For the specimen REF40-3 after interruption at t = 1,096 h and ε = 5.04%, no sliding events were observed.

The low number of sliding events found may be explained in two alternative ways. The number of sliding events is low just in Cu-OFP at longer testing times. This could contribute to the explanation why Cu-OFP has such excellent creep ductility. The other alternative is that the number of sliding events is low in both Cu-OF and Cu-OFP but that is at variance with the observed rich cavity formation in Cu-OF (Langdon 1993).

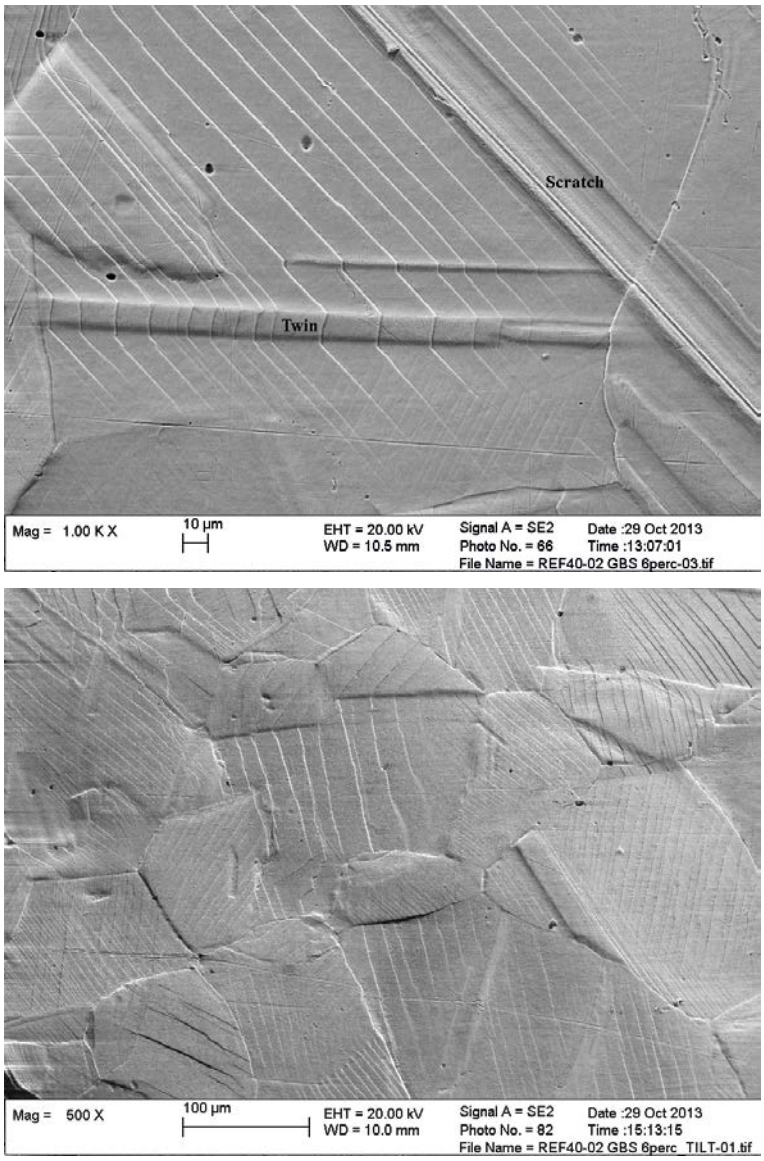

Figure 4-16. *Specimen REF40-2 at 1st interruption after t = 307 h and ε = 3.36%. SEM images showing a) scratch and slip planes, b) slip planes and bulk movement of neighbouring grains. Specimen is tilted.*

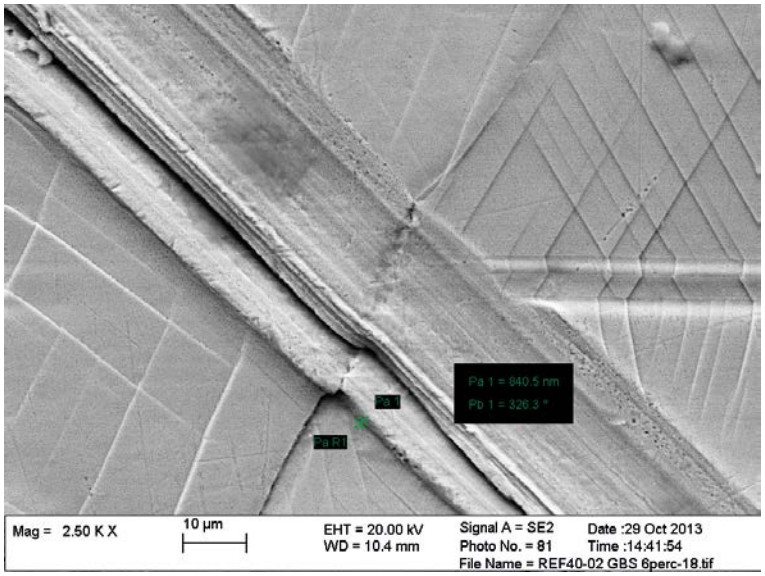

a) 0.706 µm

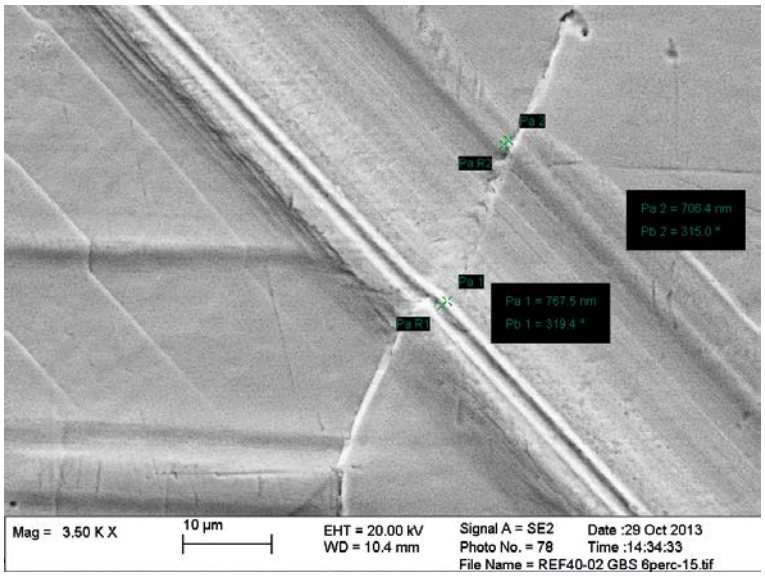

b) 0.841 µm

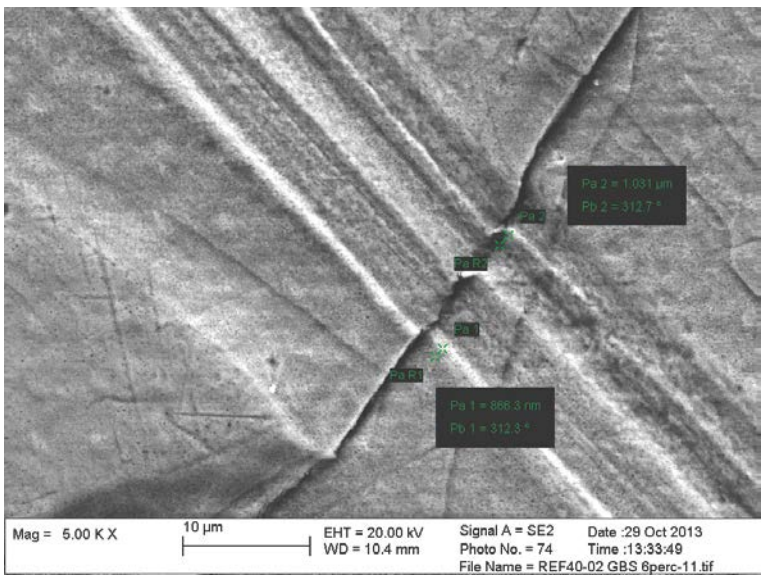

c) 0.806, 1.031 µm

Figure 4-17. *Specimen REF40-2 at 1st interruption after t = 307 h and ε = 3.36%. SEM images showing measurements of GBS.*

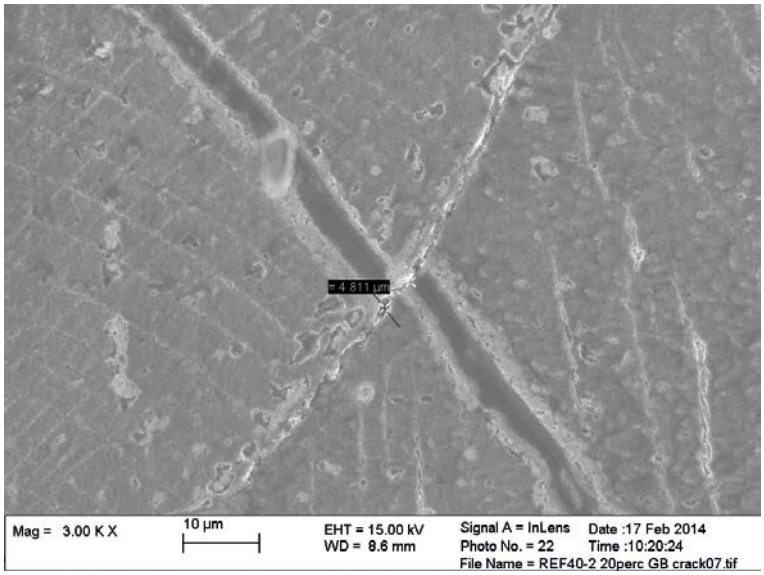

Figure 4-18. *Specimen REF40-2 at 2nd interruption after t = 507 h and ε = 20.8%. SEM images showing measurements of GBS.*

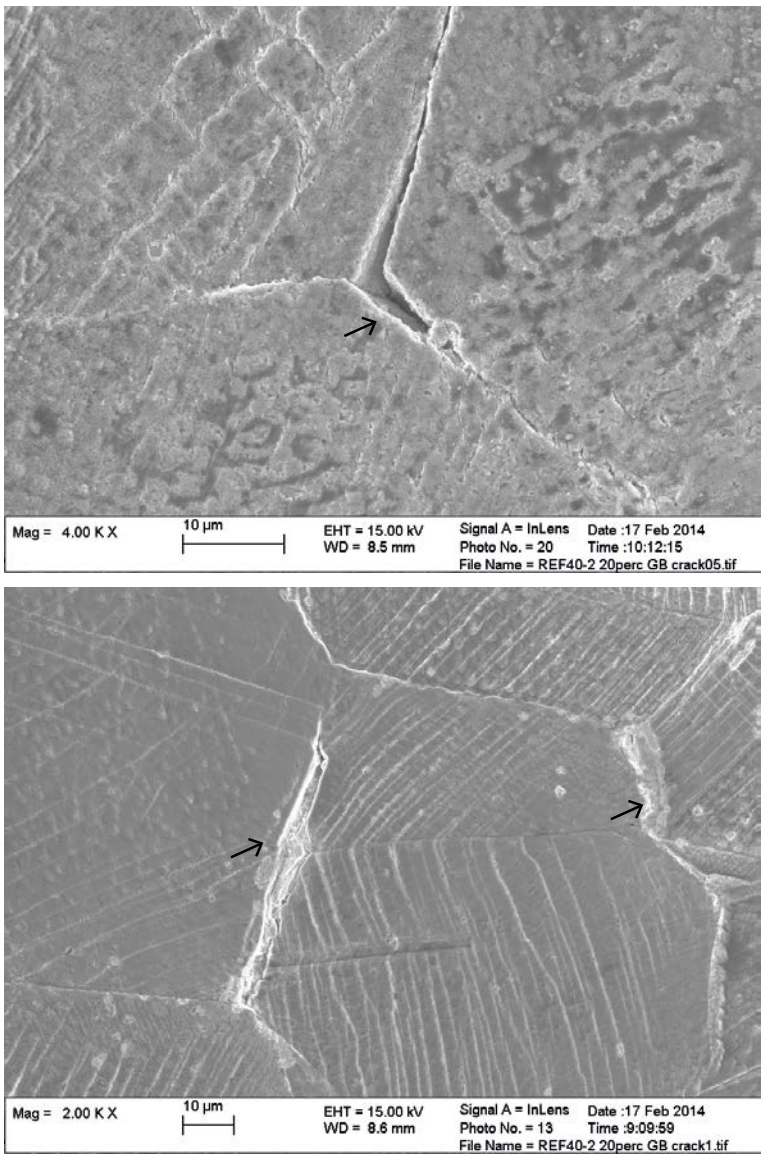

Figure 4-19. *Specimen REF40-2 at 2nd interruption after t = 507 h and ε = 20.8%. SEM images showing cracks, indicated by arrows.*

5 Discussion and analysis

5.1 Stress and strain

Stress-strain relationships were recorded continuously in the tests performed at constant loading rate. For specimen REF40-3, the results are given in Figure 4-6. After commencement of the test, strain increases slowly until a certain level of stress is reached. Further increase of stress causes faster increase of strain, indicating that the material has 'yielded'. For the test of the specimen REF40-2 before interruption, strain increases slowly with increasing stress at constant loading rate of 0.238 MPa/h. At interruption where 3.36% strain was measured at 73.7 MPa, the specimen REF40-2 was unloaded fully and temperature was reduced to room temperature in order to examine and measure GBS and to carry out an EBSD investigation. The test was then restarted from zero load at 125°C with the same constant loading rate as that before interruption. If the strain-stress curve is moved upwards as shown by the red line in Figure 4-8, it may represent the stress-strain curve without interruption. After restart, it is noticed that the strain increased faster than before the interruption even at very low stresses, see Figure 4-4 and Figure 4-8. This implies that unloading and reduction of the temperature might have softened the Cu-OFP so that 17.44% strain was accumulated already at 46.8 MPa after restart, comparing to approximately 2% strain at the same stress before interruption.

Usually, most material will be hardened if they undergo a plastic deformation due to higher dislocation density and formation of fine subgrains. The softening of the material after unloading is not well understood. It is reported that readjustment of load bar level during a creep test (corresponding to change of load) should be avoided since this action will result in additional strain accumulation (initiation of primary creep) and, in the worst case, creep specimen may fail abruptly (Wu et al. 2013). In many cases, however, the creep strain rate has been restored to that before the readjustment of the load bar level. In another study (Mannesson and Andersson-Östling 2014), the effect of load increase on creep properties is complex, depending on in which creep region (primary, secondary or tertiary creep) the load variation took place.

If a reduction of load, partially or fully, or change of temperature, or both, softens Cu-OFP, the creep performance of Cu-OFP will be significantly altered. It is possible that the creep strength of Cu-OFP will be unexpectedly decreased. Reduction (change) of load and temperature may happen as a result of earthquake and glaciation during the long-term deposition of the canister.

Creep damage may have contributed to faster strain accumulation after restart. At first interruption for the specimen REF40-2 after 307 h and 3.36% strain, no creep damage was observed. After the second interruption after 507 h and 20.8% strain, wedge cracks and intergranular cracks were found, see Figure 4-19. Many creep tests on Cu-OFP have shown that about 20% strain is frequently obtained just during uploading before the start of the actual creep test (Andersson-Östling and Sandström 2011). Creep damage in the form of cavitation can be detected at later stages of the creep test (Wu et al. 2009, Sandström and Wu 2013**)**. In the present case, many cracks were found at 20% strain, indicating that intergranular and brittle failure may occur. It is important to fully understand the effect of changes of load and temperature on creep performance of Cu-OFP material.

One interrupted-restarted-interrupted test has shown faster and larger accumulation of creep strain, implying softening of Cu-OFP. This behaviour has not been demonstrated before. To fully understand the effect of variation of load and temperature more tests and examinations must be performed.

The loading rate has obvious effects on the strain-time relation. Lower loading rate gives smaller strain due to lower strain rate, see Figure 4-7. In other words, longer time is needed to reach the same strain at lower loading rate. There seems to be a transit time over which strain increases faster even though the loading rate is constant.

Loading rate has also an effect on the strain-stress relation. At a given stress, lower loading rate produces larger strain due to creep, see Figure 4-8. There is an apparent transition, over which a faster increase in strain is seen with increasing stress. Easier deformation is believed to be a result of a change in dislocation and subgrain structure. This transition in strain-stress relation is less marked at the lower loading rate.

5.2 Grain boundary sliding

The observed amount of GBS presented in Section 4-3 is summarised in Figure 5-1.

It is commonly observed that the amount of sliding u approximately increases linearly with the creep strain ε (see e.g. Sandström and Wu 2013)

$$u = C_s\varepsilon \qquad \text{(Eq. 5-1)}$$

where C_s is a strain dependent constant. C_s can simply be obtained by dividing the displacements with the strains. The C_s values as a function of strain is presented in Figure 5-2. C_s values in the interval 20 to 65 µm were observed. The average C_s value decreases with increasing strain. It is well-known that there is significant scatter in grain boundary sliding data, and that the largest sliding does not always occur in 45° to the loading direction (Monzen et al. 1993). For this reason all significant sliding events have been recorded.

At most positions where the scratch meet the grain boundary, no measureable GBS (or shear offset) could be observed. All the same, relatively large GBS has been measured at some positions at given strains, see Figure 4-17 and Figure 4-18. However, the number of GBS which could be examined was limited and the average results are therefore subject to large standard deviations. In the specimen REF40-2 after 20.8% deformation only two sliding events were recorded. In the specimen REF40-3 no sliding events were found at all. The very low number of sliding events observed may partially explain the excellent creep ductility of Cu-OFP, since it is an indication of limited cavity formation.

In tensile tests Pettersson recorded GBS in Cu-OF and Cu-OFP at temperatures up to 200°C (Pettersson 2010). The strain rate used was 4×10^{-6} to 4×10^{-4} 1/s. The test time was up to 3 h. Ayensu and Langdon (1996) observed GBS in Cu-OF at temperatures between 400 and 600°C in short term creep tests. The strain rates were about 2×10^{-6} to 5×10^{-5} 1/s. The longest testing time was 5 h. For comparison the strain rates in the present work were in the interval 6×10^{-9} to 1×10^{-6} 1/s, see Section 4.1. In the paper of Ayensu and Langdon, the displacements are not given directly but can be derived from the following equation (Langdon 1972).

$$u = \frac{d}{\Phi}\varepsilon_{gbs} \qquad \text{(Eq. 5-2)}$$

d is the grain size, ε_{gbs} is the creep strain due to grain boundary sliding, and Φ a constant that is taken as unity.

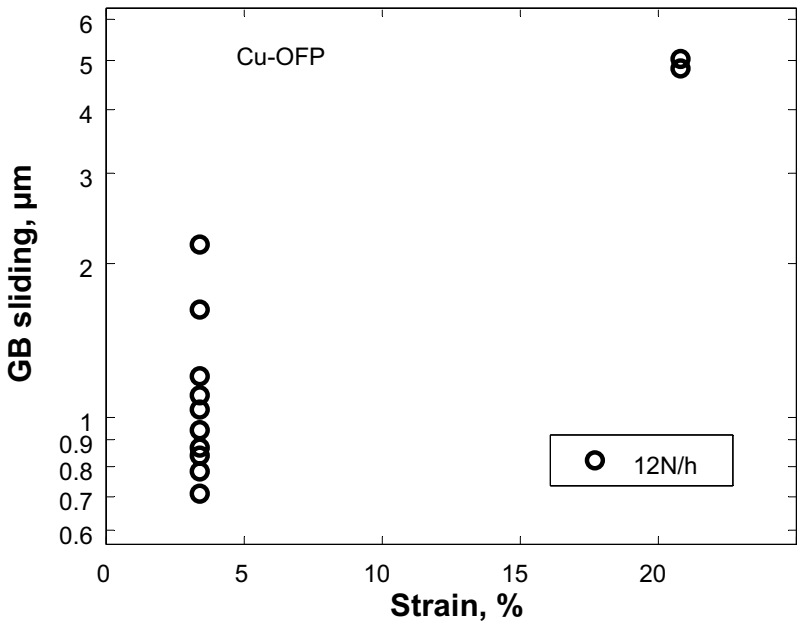

Figure 5-1. *Observed displacements at grain boundaries as a function of strain.*

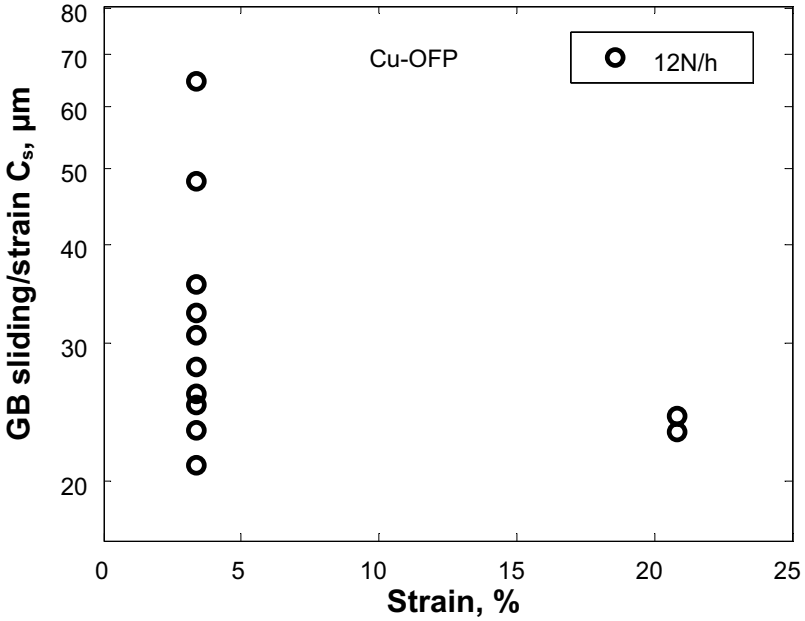

Figure 5-2. *Observed displacement divided by strain at grain boundaries (cf. Eq. 5-1).*

The results for the observed displacements from the published studies are shown together with those from the present investigation in Figure 5-3. As can be seen from the figure the displacements increase approximately linearly with strain. Pettersson's values increase slightly faster with strain than those of Ayensu and Langdon. Considering the difficulties in measuring this type of data, it can be concluded that the three investigations do not give very different results.

The ratio between the displacement and the strain for the data in Figure 5-3 is given in Figure 5-4. The C_s values which is the slope of the curves in Figure 5-3, decreases with increasing strain at least for modest strains. Again Pettersson's data are typically slightly higher than the other data. For such stochastical events as GBS, it must be considered that data lie within a fairly narrow band. In addition, the tests cover a wide range of temperatures and strain rates. Three different test types are represented in Figure 5-3 and Figure 5-4: constant stress rate, constant strain rate (tensile tests, Pettersson 2010) and constant stress (creep, Ayensu and Langdon 1996).

It is noticeable that only a limited number of sliding events were observed in the present investigation in comparison to the two published papers included in Figure 5-3. The reason may be the longer testing times and to some extent larger strains in the present study.

The decrease in the slope of the displacement versus strain curves with increasing strain has also been observed for other materials, for example for austenitic stainless steels (Kishimoto et al. 1988). However, the magnitude of the displacement for a given strain is an order of magnitude smaller than for copper.

If Eqs. 5-1 and 5-2 are combined it can be seen that the grain boundary deformation is inversely proportional to grain size for a given total strain. This means that smaller grains should give larger grain boundary sliding. Although this is likely to be the case, this is not directly supported by the experiments. The average grain size is 150 µm in the present study, 100 µm in Pettersson (2010) and 210 µm in Ayensu and Langdon (1996). However, the magnitude of Cs does not appear in this order in Figure 5-4.

An inhomogeneous grain size distribution may affect the amount of grain boundary sliding. However, there are arguments that suggest an increase and other arguments that would imply a decrease. When there is a mixture of large and small grains, the stresses on some grain boundary increase which would raise GBS. On the other hand a combination of small and large grains would lock many grain boundaries, reducing the amount of GBS. Consequently it is difficult to draw conclusions about the consequences of an inhomogeneous grain size distribution.

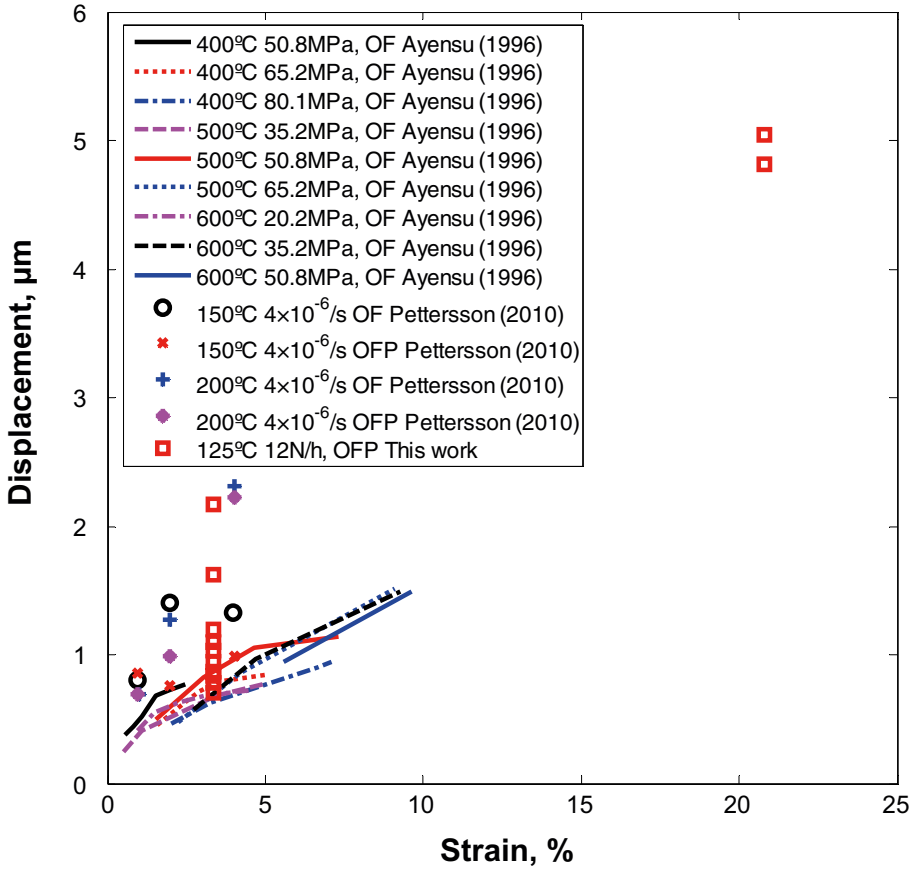

Figure 5-3. *Observed displacements at grain boundaries as a function of strain. Data from Ayensu and Langdon (1996) and Pettersson (2010) are also shown.*

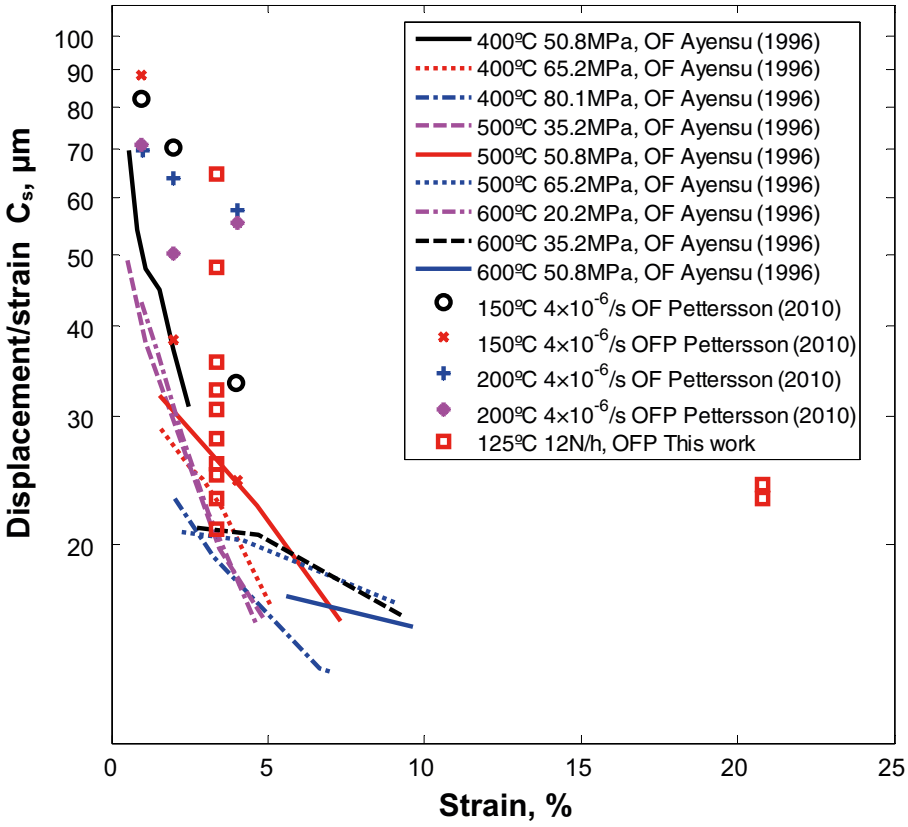

Figure 5-4. *Observed displacements at grain boundaries divided by the creep strain (cf. Eq. 5-1). Data from Ayensu and Langdon (1996) and Pettersson (2010) are also shown.*

A successful EDSB examination requires an undistorted and an oxide-free surface. After long time creep test at elevated temperature of 125°C, the surface of the tested specimen was distorted and oxidised. An electrolytic polishing method was developed and shown to work, see Figure 3-6. After electrolytic polishing, the surface was renewed, clean and smooth. This ensures a satisfactory diffraction pattern. The EDSB investigations have shown that multislip systems are active in the grains and that slip bands are formed. The dislocation density is high around the grain boundaries and small subgrains are formed there. The high dislocation density may be a result of grain rotation.

6 Conclusions

Two creep tests at 125°C with constant loading rates have been performed for as-received Cu-OFP material. The tests were interrupted before rupture. One test was restarted and interrupted again. The amount of grain boundary sliding (GBS) was measured and the changes in the microstructure due to the deformation were characterised. The following conclusions can be drawn:

1) The amount of GBS recorded was 20 to 65 μm per unit strain. This is of the same order of magnitude as in the previous studies of Ayensu and Langdon (1996) and of Pettersson (2010). Since the present study and the mentioned studies were performed with different type of deformation, it indicates that the results are not too sensitive to the mode of deformation. The three studies cover temperatures from 125 to 600°C and a range of strain rates. The results for Cu-OF and Cu-OFP are not very different.
2) The total number of observed grain boundary sliding events in the creep tests for Cu-OFP was very low.
3) For the interrupted-restarted-interrupted test, creep strain accumulated faster after restart even at very low stresses, indicating that Cu-OFP may have been softened. Influence of reduction of load and temperature during creep test on creep performance, softening behaviour in the present case, has not been previously reported. Earthquake and glaciation scenario during long-term disposal might certainly change loading conditions to which the copper canister will be exposed to, and further studies of this softening effect is therefore warranted.
4) According to the modelling, the amount of GBS is inversely proportional to the grain size. A small grain size thus enhances GBS.
5) The loading rate has obvious effects on the stress-strain-time relation. Lower loading rate causes smaller strains due to lower strain rate. At the same stress, lower loading rate produces larger strains. There is an apparent transition, over which a faster increase in strain is seen with increasing stress. This transition in strain-stress relation appears at lower stress at lower loading rate.
6) EBSD examinations validate that the Cu-OFP material has been significantly deformed. Multiple slip systems were developed in many grains. Rotation of the crystal lattice has occurred. Dislocation pile-ups induced lattice rotations at twin- and grain boundaries. Subgrains developed along the slip bands in many grains. Misorientations around 2–3° were measured.

7 Acknowledgements

This work has been performed at Swerea KIMAB. SKB is thanked for providing the testing material. Luvata Pori Oy determined the chemical analysis. Members from the research committee, Christina Lilja, Håkan Rydén, Mikael Jonsson, Matts Björck, all from SKB, and Henrik Östling, Swerea KIMAB, are thanked for discussions and comments. Facredin Seitisleam and Mats Larsson, Swerea KIMAB, are thanked for carrying out creep tests.

References

SKB's (Svensk Kärnbränslehantering AB) publications can be found at www.skb.se/publications.

Andersson-Östling H C M, Sandström R, 2011. Effect of loading rate on creep of phosphorous doped copper. SKB TR-11-09, Svensk Kärnbränslehantering AB.

ASTM E139-2011. Standard test methods for conducting creep, creep-rupture, and stress-rupture tests of metallic materials. West Conshohocken, PA: ASTM International.

Ayensu A, Langdon T G, 1996. The inter-relationship between grain boundary sliding and cavitation during creep of polycrystalline copper. Metallurgical and Materials Transactions A 27, 901–907.

Davies P W, Williams K R, 1969. Cavity growth by grain-boundary sliding during creep of copper. Metal Science 3, 220–221.

Harper J G, Shepard L A, Dorn J E, 1958. Creep of aluminium under extremely small stresses. Acta Metallurgica 6, 509–518.

Jin L-Z, Sandstrom R, 2008. Creep of copper canisters in power-law breakdown. Computational Materials Science 43, 403–416.

Jin L-Z, Sandstrom R, 2009. Non-stationary creep simulation with a modified Armstrong–Frederick relation applied to copper. Computational Materials Science 46, 339–346.

Kishimoto S, Shinya N, Tanaka H, 1988. Grain boundary sliding and surface cracking during creep of 321 stainless steel. Journal of the Society of Materials Science, Japan 37, 289–294.

Koike J, Ohyama R, Kobayashi T, Suzuki M, Maruyama K, 2003. Grain boundary sliding in AZ31 Magnesium alloys at room temperature to 523 K. Materials Transactions 44, 445–451.

Langdon T G, 1972. Effect of surface configuration on grain boundary sliding. Metallurgical Transactions 3, 797–801.

Langdon T G, 1993. The role of grain boundaries in high temperature deformation. Materials Science and Engineering A166, 67–79.

Mannesson K, Andersson-Östling H, 2014. Stress application and the effect on creep of copper. SKB R-14-31, Svensk Kärnbränslehantering AB.

Monzen R, Futakuchi M, Kitagawa K, Mori T, 1993. Measurement of grain boundary sliding of [011] twist boundaries in copper by electron microscopy. Acta Metallurgica et Materialia 41, 1643–1646.

Pettersson K, 2010. A study of grain boundary sliding in copper with and without an addition of phosphorus. Journal of Nuclear Materials 405, 131–137.

Rosborg B, Werme L, 2008. The Swedish nuclear waste program and the long-term corrosion behaviour of copper. Journal of Nuclear Materials 379, 142–153.

Rust M A, Todd R I, 2011. Surface studies of Region II superplasticity of AA5083 in shear: confirmation of diffusion creep, grain neighbour switching and absence of dislocation activity. Acta Materialia 59, 5059–5170.

Sandström R, 2012. Basic model for primary and secondary creep in copper. Acta Materialia 60, 314–322.

Sandström R, Andersson H, 2008. Creep in phosphorus alloyed copper during power-law breakdown. Journal of Nuclear Materials 372, 76–88.

Sandström R, Wu R, 2013. Influence of phosphorus on the creep ductility of copper. Journal of Nuclear Materials 441, 364–371.

Sheikh-Ali A D, 2001. Grain boundary sliding: theory. In Buschow K H J, Cahn R W, Flemings M C, Ilschner B, Kramer E J, Mahajan S, Veyssière P (eds). Encyclopedia of materials: Science and technology. 2nd ed. Oxford: Elsevier, 3624–3625.

Tan Y J, 1997. The influence of grain boundary network structure on intergranular creep cavitation of OFHC copper. MSc thesis. Department of Metallurgy and Materials Science Engineering, University of Toronto, Canada

Wu R, Jin L-Z, Sandström R, 2009. Influence of multiaxial stresses on creep properties of phosphorus alloyed oxygen free copper. In Proceedings of PVP2009, ASME Pressure Vessels and Piping Division Conference, Prague, 26–30 July 2009. PVP2009-77693.

Wu R, Sandström R, Jin L-Z, 2013. Creep crack growth in phosphorus alloyed oxygen free copper. Materials Science and Engineering A 583, 151–160.

Arkitektkopia AB, Bromma, 2016

SKB is tasked with managing Swedish nuclear and radioactive waste in a safe way.

skb.se